



# CHORUS

This is the accepted manuscript made available via CHORUS. The article has been published as:

## Morphology and Number Density of Voids in Hydrogenated Amorphous Silicon: An Ab Initio Study

Parthapratim Biswas, Durga Paudel, Raymond Atta-Fynn, David A. Drabold, and Stephen R. Elliott

Phys. Rev. Applied **7**, 024013 — Published 13 February 2017

DOI: [10.1103/PhysRevApplied.7.024013](https://doi.org/10.1103/PhysRevApplied.7.024013)

# Morphology and number density of voids in hydrogenated amorphous silicon: an ab initio study

Parthapratim Biswas\* and Durga Paudel

*Department of Physics and Astronomy, The University of Southern Mississippi, Hattiesburg, MS 39406<sup>†</sup>*

Raymond Atta-Fynn<sup>‡</sup>

*Department of Physics, University of Texas, Arlington, TX 76019*

David A. Drabold<sup>§</sup>

*Department of Physics and Astronomy, Ohio University, Athens, OH 45701*

Stephen R. Elliott<sup>¶</sup>

*Department of Chemistry, University of Cambridge, Cambridge, CB2 1EW, United Kingdom*

We present a first-principles study of the formation and structure of microvoids in device-quality models of hydrogenated amorphous silicon (*a*-Si:H). Using a combination of classical metadynamics and first-principles density-functional calculations, which is capable of generating large *a*-Si:H models with a linear size of several nanometers and a realistic hydrogen distribution, we have examined the morphology and computed the number density of microvoids at low and high concentrations of hydrogen. The results of our calculations are compared with experimental data from SAXS, and hydrogen and implanted-helium effusion measurements. Our study suggests that the number density of microvoids is of the order of  $7\text{--}8 \times 10^{18} \text{ cm}^{-3}$  for device-quality models with 8–10 at. % H, and which increases to  $1\text{--}3 \times 10^{19} \text{ cm}^{-3}$  with an increase of hydrogen content to 18 at. %. The morphology of the microvoids has been found to be highly complex with a radius of gyration varying from 2.7 Å to 5.0 Å for very large models. The spatial distributions of microvoids at low and high concentrations are strongly influenced by the presence of isolated and interconnected voids, respectively, which are consistent with the results from hydrogen and implanted-helium effusion measurements. The simulation methodology and results presented here have direct applications in large-scale modeling of *a*-Si:H/*c*-Si heterojunctions with intrinsic thin-layer technology for the development of next-generation silicon solar cells and resistive switching mechanisms in ultra-low-power non-volatile memory devices, such as chalcogenide- or oxide-based conductive bridging random access memory (CBRAM) devices.

## I. INTRODUCTION

Hydrogen plays an important role in determining the electronic and optical properties of hydrogenated amorphous silicon (*a*-Si:H). Since pure amorphous silicon (*a*-Si) has too many coordination defects ( $\sim 10^{20} \text{ cm}^{-3}$ ) to be useful as a device material, the addition of a small quantity of hydrogen in *a*-Si passivates the dangling bonds and improves the electronic and optical responses by reducing its defect density. The presence of too much hydrogen (above 10–12 at. %), however, can induce significant structural changes in *a*-Si:H through the formation of silicon-hydrogen bonding complexes and these have been observed using nuclear magnetic resonance (NMR)[1, 2] and infrared (IR) spectroscopy.[3, 4] Hydrogen also plays a crucial role in the light-induced degradation of *a*-Si:H through the creation of metastable defects, such as mobile H complexes[5] and additional dangling bonds produced upon illumination.[6]

Experimental probes, which can measure the hydrogen content and evolution of the hydrogen concentration profile in *a*-Si:H, such as infrared (IR)[3, 7] and secondary ion mass

spectrometry (SIMS),[8] respectively, suggest that approximately 3–4 at. % H can reside in the *a*-Si:H matrix as isolated monohydrides.[7] Upon further addition of hydrogen, clusters of mono- and dihydride bonds begin to appear and, at very high concentration, hydrogen molecules form inside small microvoids.[8] It is widely accepted that hydrogen atoms bonded to silicon atoms on the void surfaces can desorb to form H<sub>2</sub> molecules, the presence of which can be inferred, directly or indirectly, from NMR [9], calorimetry [10, 11] and IR [12] measurements. The formation of H<sub>2</sub> molecules introduces dangling or weakly-reconstructed Si bonds on the void surfaces, which produce defect states that adversely affect the electronic and optical properties of the material. Carlson[6] and others[13, 14] have proposed that hydrogenated voids play a key role in the light-induced degradation of *a*-Si:H by trapping holes near the internal surface of the voids, and the recent experiment on *a*-Si:H using time-domain pulsed electron paramagnetic resonance (EPR) spectroscopy by Fehr *et al.*[15] appears to confirm this proposition. Since small-angle X-ray scattering (SAXS) [16, 17] conclusively demonstrates the existence of voids in device-quality *a*-Si:H, it is important to understand the role of microvoids in determining the microstructure of the hydrogen distribution in *a*-Si:H. To this end, the main purpose of the paper is to present a morphological study of microvoids with an emphasis on the computation of the density of microvoids for varying concentrations of hydrogen. Here, we employ a recently-developed computational technique, [18] which can produce large models

---

\* partha.biswas@usm.edu; Corresponding Author

† durga.paudel@usm.edu

‡ attafynn@uta.edu

§ drabold@ohio.edu

¶ sre1@cam.ac.uk

of  $a$ -Si:H on the several nanometer length scale with varying hydrogen contents, by using a combination of classical metadynamics and first-principles density-functional simulations. Using these models as the structural basis, we address the morphology and spatial distribution of microvoids, and compare the results with the same from SAXS,[16, 17] IR,[3, 4, 7] and gas-effusion measurements using hydrogen and implanted helium.[19–21]

The rest of the paper is organized as follows. In section II, we have provided a brief description of the morphology of voids obtained from SAXS, positron annihilation spectroscopy (PAS), and gas-effusion measurements. Section III addresses the implementation of the computational method that comprises classical metadynamics simulations involving an appropriate configuration constraint to incorporate the correct environment of silicon-hydrogen bonding configurations into simulations, hydrogen passivation and *ab initio* relaxation of the resulting hydride configurations. The structural, topological and electronic properties of the models are examined, and the morphology of the voids are discussed in section IV with an emphasis on the density of microvoids and their microstructural distribution in real space for different concentrations of hydrogen. A comparison of the simulated SAXS intensity obtained from our models with that from experiments is also provided in this section. The conclusions of the work are presented in Section V with an emphasis on the application of our method and analysis to the development of  $a$ -Si:H/ $c$ -Si-based heterojunction solar cells and ultra-low-power resistive switching random access memory (ReRAM) devices.

## II. EARLIER WORKS: AN OVERVIEW

Experimentally, the presence of voids in  $a$ -Si:H has been studied extensively using an array of methods ranging from SAXS,[16, 17] IR spectroscopy,[3, 4, 7, 12] PAS [22] and effusion measurements[19, 20] of hydrogen and implanted helium. The morphology of microvoids in  $a$ -Si:H has been observed to be too complex to be determined reliably from SAXS or IR results alone. Since SAXS results are typically interpreted using the Guinier approximation,[23] which assumes a homogeneous distribution of cavities or density-deficient regions on a length scale of several nanometers, it is difficult to detect accurately the presence of small microvoids with a linear size of a few angstroms using SAXS only. Likewise, hydrogen effusion alone cannot detect the difference between isolated and interconnected voids in  $a$ -Si:H.[19] Nonetheless, an analysis of experimental data from SAXS,[16, 17] IR,[12] and effusion measurements[19, 20] of hydrogen and implanted helium has led to the conclusion that even device-quality films of  $a$ -Si:H contain a small amount of microvoids, depending upon the preparation methods and conditions, and the concentration of hydrogen in the samples. By combining SAXS data with IR measurements, Williamson *et al.*[24] have observed that the number density of microvoids in device-quality glow-discharge-deposited  $a$ -Si:H films can vary from  $2 \times 10^{19}$  to  $4.9 \times 10^{19}$   $\text{cm}^{-3}$ , and the radius of gyration ranges from 3.3 Å to 3.9 Å. These results are con-

sistent with the SAXS data obtained by Mahan *et al.*[17] from device-quality glow-discharge  $a$ -Si:H and  $a$ -Si $_{1-x}$ C $_x$ :H, where the gyration radii of microvoids have been found to be in the range 3.3–4.8 Å with a volume fraction of voids as low as 0.01 in device-quality  $a$ -Si:H and 0.2 in non-device quality films obtained at low substrate temperatures.[17] Muramatsu and coworkers[22] have employed PAS to study  $a$ -Si:H samples obtained from radio-frequency (RF) and plasma-enhanced chemical vapor deposition (PECVD) methods, and concluded that the typical microvoid volume ranges from 50 Å<sup>3</sup> to 60 Å<sup>3</sup>. This approximately translates into a linear size of 3.7–3.9 Å. The morphology of microvoids in device-quality undoped plasma-grown  $a$ -Si:H has been studied by Beyer *et al.*[19, 20] as a function of the substrate temperature and hydrogen content using hydrogen and implanted-helium effusion measurements. The results indicate that interconnected voids are a characteristic feature of the hydrogen microstructure, which generally appear at a high hydrogen concentration (above 15–20 at. % H), and are associated with low substrate temperatures. Isolated voids, on the other hand, have been observed to be present at a low concentration (below 10–12 at. % H) and have an approximate density of  $10^{18}$   $\text{cm}^{-3}$ . The inert nature of He atoms suggests that the trapped He atoms inside isolated cavities can only be released at high temperature (and with a consequent increase of pressure within the cavities) via a permeation process.[20]

## III. COMPUTATIONAL METHOD

The discussion in the preceding section suggests that, in order to study microvoids in model  $a$ -Si:H networks, one must be able to simulate very large models with a linear size of several nanometers. Additionally, since voids are intrinsically related to the distribution of hydrogen, the approach should also be able to produce a reliable hydrogen distribution in order to facilitate the formation of voids in the networks. *Ab initio* molecular dynamics (AIMD) appears to be a natural choice to address this but, given the computational complexity of the problem involving several thousand atoms, a direct application of AIMD has proved to be too expensive and impractical. On the other hand, since large-scale modeling of high-quality  $a$ -Si networks can be done in various ways[25–27] using classical potentials,[28] a pragmatic approach to generate a realistic hydrogen distribution would be to produce large  $a$ -Si networks with customized defect configurations in controlled quantities via biased dynamics coupled with appropriate geometrical or configurational constraints. It has been shown recently that geometrical[29] and electronic[30] constraints can be used very profitably, not only to generate high-quality configurations of amorphous semiconductors but also to control their electronic properties by including constraint forces in stochastic[27] and biased molecular-dynamics simulations.[30] Following this philosophy, we employ metadynamics to produce specific coordination defects by incorporating a configuration-constraint parameter  $Z$  for the production of device-quality models of  $a$ -Si:H. We define  $Z = N_{\text{SiH}}^{\text{iso}} / \sum_n N_n$ , where  $N_n$  is the number of SiH $_n$  con-

figurations with  $n = 1, 2$  and  $3$ , and  $N_{SiH}^{iso}$  is the number of isolated Si-H bonds. By controlling  $N_n$  via metadynamics sampling,[18] it is possible to generate device-quality *a*-Si:H models with appropriate amounts of isolated Si-H bonds as observed in experiments.[7, 8] Below, we briefly describe our method. The reader may refer to Ref. 31 for details.

We began with a random configuration of 6000 Si atoms in a cubic simulation cell ( $\approx 51 \text{ \AA} \times 51 \text{ \AA} \times 51 \text{ \AA}$ ) and con-

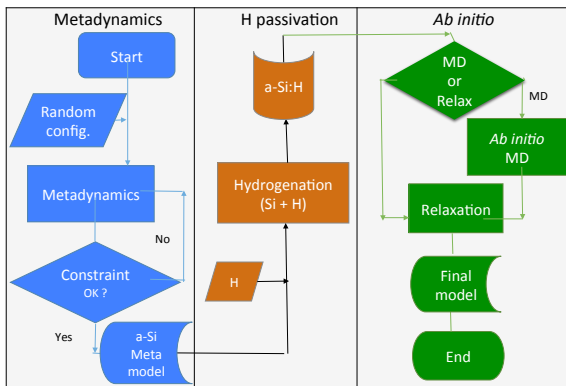


FIG. 1. (Color online) A flow diagram showing the key steps of the method. The computational steps associated with metadynamics simulations, hydrogen passivation and *ab initio* relaxations are shown in blue, brown and green colors, respectively.

ducted constant-temperature classical MD simulations using the modified Stillinger-Weber potential.[28] The temperature of the system was controlled by a chain of Nosé-Hoover thermostats.[32] Initially, the system was equilibrated at 1700 K for 200 picoseconds. The temperature of the system, then, was reduced in steps by 300 K, followed by equilibration for 200 picoseconds at that temperature, until the final temperature was 500 K. Thus, the total simulation time for the MD runs was 1 nanosecond in this work. Once the constant-temperature run at 500 K was completed, a gaussian bias potential was switched on to initiate the *metadynamics* simulation. Metadynamics is essentially a biased molecular-dynamics method for rapid sampling of the free-energy surface (FES) characterized by a set of collective variables. In the present work, we used a continuous near-neighbor function as the collective variable to produce an ensemble of low-energy configurations on the FES.[33] We generated an ensemble of configurations via metadynamics, and selected those with under-coordinated Si atoms only. Each selected configuration was further examined on the fly to ensure that the configuration had a requisite number of isolated 3-fold or dangling bonds in order to produce 3–5% isolated monohydrides upon hydrogenation. This was achieved by using the configuration-constraint parameter  $Z$ . Hydrogenation of the selected configurations proceeded by adding H atoms at the defect sites

following the prescription outlined in Ref. 31. To generate reliable statistics, we studied two sets of *a*-Si:H configurations: five independent configurations with concentrations of 8.3–9.3 at. % H and five independent configurations with concentrations of 18.2–18.4 at. % H.

Once the hydrogenation was completed, the total energy of each of the resulting ten hydride configurations was minimized using the density functional theory (DFT), as implemented in the electronic-structure package SIESTA.[34] The DFT implementation in SIESTA is based on atom-centered basis functions and norm-conserving pseudopotentials for electron-ion interactions. The Perdew-Zunger formulation of the local density approximation (LDA) to the exchange-correlation functional[35] was employed in this work. The norm-conserving pseudopotentials used in this work were based on the Troullier-Martins scheme [36], which were modified into a separable form due to Kleinman and Bylander.[37] The valence-electron states were expanded using double- $\zeta$  localized basis functions.[38] Owing to the large size of the models (and the use of double- $\zeta$  basis), the Kohn-Sham equations were solved non-self-consistently using the Harris-functional approach[39], and only the  $\Gamma$  point in the  $k$  space was used in our calculations. Given the computational complexity of the problem and the modest size of the cell—indicating the collapse of the Brillouin zone into a point ( $\Gamma \approx 0$ )—these are reasonable approximations for our purpose. Earlier studies have indicated that, to obtain converged energetics for H, a full self-consistent electronic calculation is necessary along with an extended basis set for Si and H atoms.[40] Our problem is somewhat different: we are mostly concerned here with the statistical aspect of the morphology of voids and the character of H-bonded silicon atoms associated with the voids. We will see in section IV that all indications are there that our approximations are adequate for this, especially when compared to experiments.[18] The total energy of each configuration was minimized by simultaneously relaxing the atomic positions and cell vectors with the convergence criteria: (i) the maximum atomic force on an atom along each coordinate direction was less than 0.04 eV/Å; and (ii) the cell stress was less 0.1 GPa. A schematic diagram showing the key steps of the method is presented in Fig. 1.

## IV. RESULTS AND DISCUSSION

### A. Structural and electronic properties

Before addressing the results, we first establish that the key structural and electronic properties of *a*-Si:H, as well as the characteristic features of the H distribution, are correctly reproduced by our models. In Table I, we have listed the key properties of the models: size ( $N$ ), hydrogen content ( $C_H$ ), mass density ( $\rho$ ), average bond angle ( $\theta$ ) and its standard deviation ( $\Delta\theta$ ), and the percentage of 4-fold coordinated Si atoms ( $C_4$ ) in the networks. The last three quantities suggest that the *a*-Si:H networks are highly tetrahedral in character with an average bond angle of  $109.2^\circ \pm 9.4^\circ$  and have coordination defects less than 0.2%. The concentration of H atoms in var-

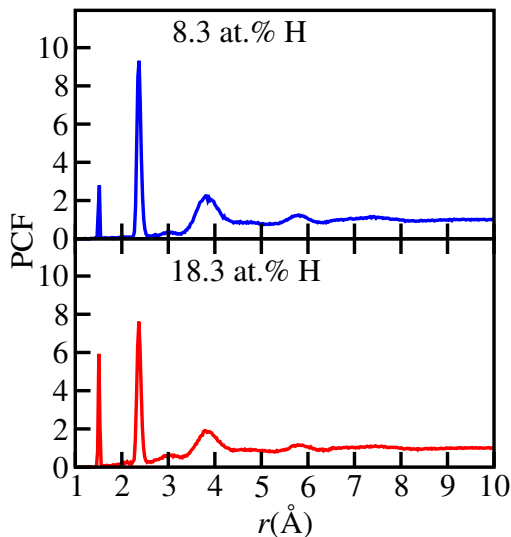


FIG. 2. Pair-correlation functions (PCF) for  $a$ -Si:H from two models: a) 8.3 at. % H and b) 18.3 at. % H of hydrogen as indicated. For clarity, the featureless regions beyond 10.0 Å are omitted in the plot.

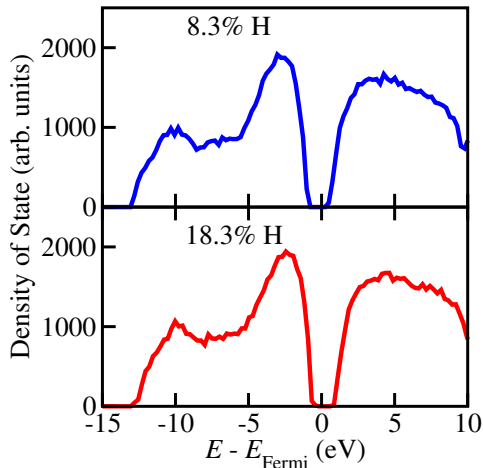


FIG. 3. Electronic density of states from two models of  $a$ -Si:H with H concentration as indicated. The valence- and conduction-band regions and the size of the electronic gap are correctly produced here.

ious silicon-hydrogen bonding configurations is also listed in Table I. A real-space analysis of the models suggests that approximately  $4.2 \pm 1.8$  % of the total H atoms at low concentration are distributed in the network as isolated SiH bonds, where the Si-bonded H atom does not have any H neighbor within a radius of 5 Å. This result is consistent with the experimental data from SIMS [8] and IR spectroscopy[7]. Table I also confirms that, at high concentration of hydrogen, H atoms begin to form more and more SiH<sub>2</sub> and SiH<sub>3</sub> configurations, which affect the H microstructure as observed in NMR[1] and IR measurements,[3, 4, 7] and in our earlier computational studies.[41, 42] The radial pair-correlation functions at low and high concentrations are shown in Fig. 2. The plot shows the characteristic presence of the peaks at 1.5 Å and 2.38 Å, which indicate the bond length of Si-H and Si-Si bonds, re-

TABLE I. Structural properties of  $a$ -Si:H models.  $N$ ,  $C_H$ ,  $\rho$ ,  $\theta$ ,  $\Delta\theta$  and  $H_{\text{Iso}}$  are the number of atoms, hydrogen content (at. %), atomic mass density ( $\text{gm.cm}^{-3}$ ), average bond angle (degree) and its standard deviation, and the percentage of isolated monohydrides (w.r.t the total monohydrides), respectively.  $C_4$  is the concentration (in %) of 4-fold coordinated Si atoms and  $M_X$  is the fraction of H atoms distributed in  $X=\text{SiH}_n$  bonding configurations.  $M_X = \left[ \frac{nN_n}{N_h} \right]$ , where  $N_n$  and  $N_h$  are the total number of SiH<sub>n</sub> ( $=X$ ) configurations and H atoms, respectively.

| $N$                | $C_H$ | $\rho$ | $H_{\text{Iso}}$ | $\theta$ | $\Delta\theta$ | $C_4$ | $M_{\text{SiH}}$ | $M_{\text{SiH}_2}$ | $M_{\text{SiH}_3}$ |
|--------------------|-------|--------|------------------|----------|----------------|-------|------------------|--------------------|--------------------|
| Low Concentration  |       |        |                  |          |                |       |                  |                    |                    |
| 6544               | 8.3   | 2.212  | 7.8              | 109.2    | 9.32           | 99.93 | 0.9              | 0.1                | 0                  |
| 6558               | 8.5   | 2.210  | 3.4              | 109.2    | 9.33           | 99.82 | 0.886            | 0.104              | 0.01               |
| 6616               | 9.3   | 2.206  | 3.0              | 109.2    | 9.39           | 99.98 | 0.919            | 0.081              | 0                  |
| 6574               | 8.7   | 2.209  | 4.0              | 109.2    | 9.29           | 99.98 | 0.906            | 0.094              | 0                  |
| 6582               | 8.8   | 2.209  | 2.6              | 109.2    | 9.36           | 99.95 | 0.925            | 0.075              | 0                  |
| High Concentration |       |        |                  |          |                |       |                  |                    |                    |
| 7342               | 18.3  | 2.158  | 0.3              | 109.1    | 9.60           | 99.91 | 0.755            | 0.225              | 0.02               |
| 7346               | 18.3  | 2.165  | 0                | 109.1    | 9.69           | 99.82 | 0.765            | 0.213              | 0.022              |
| 7344               | 18.3  | 2.156  | 0.4              | 109.1    | 9.67           | 99.90 | 0.769            | 0.20               | 0.031              |
| 7338               | 18.2  | 2.159  | 0.2              | 109.1    | 9.70           | 99.88 | 0.767            | 0.22               | 0.013              |
| 7352               | 18.4  | 2.160  | 0.1              | 109.1    | 9.66           | 99.98 | 0.746            | 0.218              | 0.036              |

spectively. To further validate the models, we have plotted in Fig. 3 the electronic density of states (EDOS) for two models of  $a$ -Si:H obtained from the density-functional package SIESTA in the local density approximation. The EDOS produces a clean electronic gap of 1.3–1.4 eV, which is consistent with the narrow bond-angle distribution, a few coordination defects, and the limitation of the local density approximation associated with density-functional calculations.

## B. Density of microvoids in $a$ -Si:H

The determination of the microvoid density in  $a$ -Si:H networks, with a linear size of several nanometers, is a non-trivial task owing to the presence of interstitial space in the network. Since we are primarily interested in finding the centers of cavities or microvoids, and not the trivial atomic-interstitial regions in  $a$ -Si:H, we employ the method developed in Ref. 43. The method is capable of identifying small microvoids in amorphous networks by partitioning the 3-dimensional model network into atomic, interstitial and cavity or microvoid regions. The morphology of the microvoids can be identified by discretizing the space into small cubic volume elements or *voxels*, and determining those voxels that do not belong to the atomic and interstitial regions. By identifying a set of connected voxels (i.e. a voxel cluster), one can approximate a microvoid region by a cluster. The volume and radius of gyration of a microvoid follow from the corresponding cluster consisting of individual voxels. The microvoid shape can be obtained from the constituent voxels and it can be visualized

TABLE II. Microvoid density in model  $a$ -Si:H networks at low and high H concentrations.  $R_g$ ,  $C_H$ ,  $\rho_v$  and  $\delta v$  stand for the radius of gyration ( $\text{\AA}$ ), hydrogen content (at. % H), density of voids ( $\text{cm}^{-3}$ ) and the percentage of void volume in  $a$ -Si:H, respectively. The Manhattan radius ( $R_L$ ) ( $\text{\AA}$ ) is indicated next to the  $R_g$  values within parentheses.

| $N$                | $C_H$ | $\rho_v$              | $R_g(R_L)$  | $\delta v$ |
|--------------------|-------|-----------------------|-------------|------------|
| Low Concentration  |       |                       |             |            |
| 6544               | 8.3   | $7.88 \times 10^{18}$ | 2.53 (3.54) | 1.39       |
| 6558               | 8.5   | $7.87 \times 10^{18}$ | 2.94 (3.68) | 1.25       |
| 6616               | 9.3   | $7.85 \times 10^{18}$ | 2.78 (3.75) | 1.5        |
| 6574               | 8.7   | $7.87 \times 10^{18}$ | 2.75 (3.83) | 1.42       |
| 6582               | 8.4   | $7.86 \times 10^{18}$ | 2.58 (3.69) | 1.22       |
| High Concentration |       |                       |             |            |
| 7342               | 18.3  | $1.53 \times 10^{19}$ | 3.21 (4.5)  | 3.53       |
| 7346               | 18.3  | $2.30 \times 10^{19}$ | 2.83 (3.99) | 3.72       |
| 7344               | 18.3  | $1.52 \times 10^{19}$ | 2.68 (3.75) | 2.60       |
| 7338               | 18.2  | $3.06 \times 10^{19}$ | 2.98 (4.20) | 5.7        |
| 7352               | 18.4  | $1.53 \times 10^{19}$ | 3.92 (5.27) | 3.38       |

using a suitable 3-dimensional volume-rendering software. A detailed description of the method is given elsewhere.[43] In Table II, we have listed the density of microvoids at low and high concentrations of hydrogen for five independent  $a$ -Si:H configurations. To calculate the density of voids, we have chosen an effective cutoff radius of  $2.0 \text{ \AA}$  for the clusters. Clusters with a radius of gyration smaller than  $2.0 \text{ \AA}$  are not counted in the calculations to ensure that the empty regions associated with isolated mono-vacancies and any spurious cavities are excluded from our estimates. Table II shows that the density of microvoids at a low concentration (of 8.3 at. % H) is of the order of  $8 \times 10^{18} \text{ cm}^{-3}$  with a volume fraction of voids from 0.012 to 0.015. These values are comparable with the experimental void density of  $2\text{--}4.5 \times 10^{19} \text{ cm}^{-3}$  and void-volume fraction 0.010–0.015 reported by Williamson *et al.*[24] from a combination of SAXS and IR measurements on device-quality samples. The computed values of the radius of gyration ( $R_g$ ) in our work have been found to be in the range  $2.5\text{--}3.9 \text{ \AA}$ , which are somewhat smaller than the experimental values of  $3.3$  to  $3.9 \text{ \AA}$ . [24] However, this deviation from experimental data is not surprising and can be attributed partly to the aggressive elimination of atomic-interstitial volumes for the construction of microvoid regions, and in part to the use of the Guinier approximation[23] in the determination of  $R_g$  values from experimental SAXS data. Since computer models, with a linear dimension of a few nanometers, may not adequately satisfy the Guinier limit, the  $R_g$  values obtained from our models are affected by finite-size effects, and provided a lower bound of the microvoid radii. In addition to the conventional average radius of gyration, we have also examined other linear measures to estimate the size of the microvoids. For example, the  $L^1$ -norm or Manhattan radius[44] provides a simple measure of the linear dimension of the microvoids, which is particularly suitable here for analyzing microvoid

clusters distributed over a cubic grid. The average Manhattan radius  $R_L$  of the microvoids is indicated in Table II next to the  $R_g$  values, which is in the range of  $3.5\text{--}5.3 \text{ \AA}$ . Finally, as an additional check, our results can be compared with the experimental values of the number density of voids obtained from gas-effusion measurements. Effusion measurements of

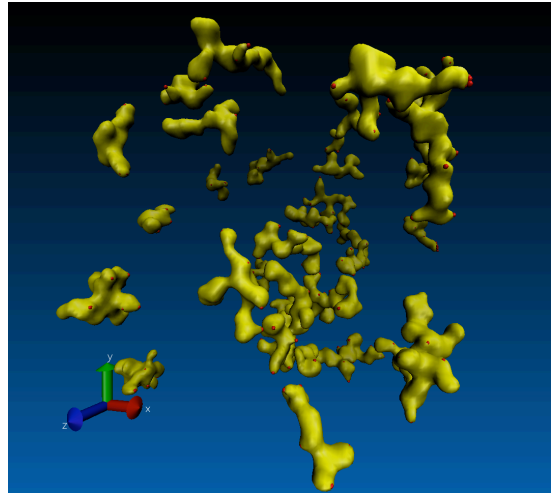


FIG. 4. Microvoid distribution in an  $a$ -Si:H model with 8.3 at. % H. The solid yellow blobs represent the outer surface of the microvoids showing an almost isolated distribution of voids.

hydrogen and implanted helium by Beyer *et al.*[19, 20] suggest that the density of voids lies in the range  $2\text{--}3 \times 10^{18} \text{ cm}^{-3}$  in device-quality  $a$ -Si:H samples (10 at. % H) obtained at low substrate temperatures near  $200 \text{ }^\circ\text{C}$ . Thus, the computed values of the number density from our models are intermediate between the experimental values from SAXS and IR, and those from the effusion measurements on device-quality samples. The number density for the models with a high concentration of hydrogen (18.3 at. % H) is also listed in Table II. The number density and void-volume fraction in this case have been found to be approximately two or three times larger than that in device-quality models. This observation is on a par with our expectation and it is supported by gas effusion and SAXS measurements,[17, 20, 21] which indicate that, at high concentrations (of H), the microstructure of H distribution is significantly modified through the formation of clusters of SiH/SiH<sub>2</sub> bonds. This increases the probability of microvoid formation via desorption of H atoms from weak SiH/SiH<sub>2</sub> bonding complexes, and facilitates the formation of small cavities with a few H<sub>2</sub> molecules inside.

### C. Morphology of voids in $a$ -Si:H: isolated and interconnected distributions

Having addressed the density of voids in  $a$ -Si:H, we now examine the morphology and characteristic features of the void distributions as a function of hydrogen content. Experimental data from IR,[12], NMR,[1] and calorimetry[10] measurements, and computer simulations of  $a$ -Si:H,[41, 42]

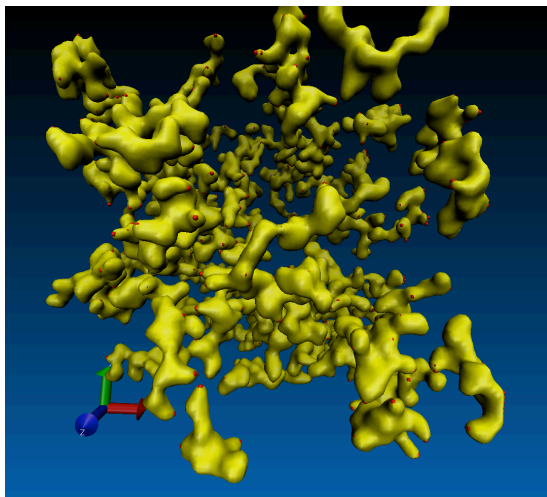


FIG. 5. A highly interconnected distribution of microvoids observed in a model *a*-Si:H network with 18.3 at. % H. An agglomeration of a large number of clusters of varying sizes has produced several interconnected regions as shown by the yellow blobs.

which provide useful information on the microstructure of hydrogen distribution, suggest that voids can be distributed in the network in an isolated or interconnected way, depending upon the preparation methods, experimental conditions, and the amount of hydrogen in the network. Effusion measurements of hydrogen and helium provide a clear picture on the distribution of voids in *a*-Si:H. Beyer and coworkers[19, 20] have observed that helium effusion can distinguish interconnected voids from isolated ones unambiguously as the presence of the former show up in low-temperature He-effusion measurements. In contrast, isolated voids can be detected only at high temperature when the sporadically trapped He atoms leave the cavities by a permeation process at high temperature and with a consequent rise of the pressure inside the cavities.[45] Although the density of interconnected voids has been found to decrease upon annealing of the samples[20, 21]—possibly due to thermal diffusion of H atoms or otherwise—interconnected voids continue to prevail at high concentration, as indicated by the strong dependence of the He-effusion peak temperature with hydrogen content.[19] Since the *a*-Si:H models studied in this work are obtained by local relaxations of the structure upon hydrogenation, which do not incorporate the effect of thermal motion of H atoms on the hydrogen distribution in the networks, it is appropriate to compare these models with *as-deposited* samples of *a*-Si:H. Thus, we should expect a strong presence of interconnected voids at high concentration and isolated voids at low concentration of hydrogen. The spatial distribution of microvoids for the models with 8.3 at. % H and 18.3 at. % H are presented in Fig. 4 and 5, respectively. To minimize the effect of spurious empty regions on the void distribution, we have chosen only the clusters with a minimum volume of 25 Å<sup>3</sup> or above. This value is close to the observed void volume of 40–60 Å<sup>3</sup> obtained from PAS,[22] and is useful to separate non-trivial microvoid regions from any possible artifacts that

might have been produced by our method. Figure 4 shows the distribution of several isolated void regions, the shapes of which are highly complex and far from being spherical. The shape of a microvoid has been constructed by enveloping the corresponding cluster with a gaussian surface, which is mathematically equivalent to the convolution of a voxel cluster with a 3-dimensional gaussian function. Physically, this represents the ‘blurring’ of a cluster by a gaussian function. Figure 5 clearly reveals that at a high concentration of 18.3 at. % H, the number density of voids has increased considerably and several small microvoid regions have coalesced into an interconnected region. We should mention that the shape and degree of connectivity between the voids regions depend, to an extent, on the linear size ( $\Delta x$ ) of the voxels.[46] A choice of  $\Delta x = 0.5\text{--}0.6$  Å has been found to work satisfactorily for our work. This value is somewhat larger than the diameter of H atoms.

Since SAXS and voids are intimately related to each other, we now briefly address the computation of the SAXS intensity as a function of the magnitude of the scattering vector for a model *a*-Si:H network and compare the same with the experimental SAXS data. The scattering intensity for a network consisting of  $N$  identical atoms can be written as,[47]

$$I(\mathbf{s}) = \sum_{i=1}^N \sum_{j=1}^N f_i(s) f_j(s) \exp [i \mathbf{s} \cdot (\mathbf{r}_i - \mathbf{r}_j)]. \quad (1)$$

Here the magnitude of the scattering vector  $\mathbf{s}$  is given by  $s = |\mathbf{k} - \mathbf{k}_0| = (4\pi/\lambda) \sin \theta$ , where  $\mathbf{k}_0$  and  $\mathbf{k}$  are the wavevectors of the incident and diffracted beams, respectively, and  $2\theta$  is the (scattering) angle between the two vectors. The atomic-scattering factor of the atom at the site  $i$  is given by  $f_i(s)$ , which is, in general, a function of  $s$  but can be considered as constant for very small values of  $s$ . While the evaluation of the double sum appears to be rather straightforward, the main difficulty arises in the computation of the average value of  $I(\mathbf{s})$  for a large but finite system, especially in the presence of periodic boundary conditions when the double sum in Eq. 1 cannot be decoupled and replaced by the square of a single sum.[48] In the conventional treatment of bulk disordered systems, the configuration averaging is performed analytically by assuming: 1) the atomic distribution is isotropic; 2) a normalized radial probability distribution function  $P(r_{ij})$  can be defined to describe the probability of finding an atom at  $r_j$ , given that there is an atom at  $r_i$ ; and 3) the scattering contribution from a term involving a constant density, which is proportional to  $\sin(sr_{ij})/sr_{ij}$  and corresponds to the scattering from a particle of volume  $V = L^3$  or the entire system, can be neglected for the vectors  $s > 2\pi/L$ , where  $L$  is the linear size of the model. [47] This leads to the classical expression of Zernike and Prins,[50]

$$I(s) = N f^2(s) \left[ 1 + \frac{4\pi N}{V} \int_0^\infty (P(r) - 1) \frac{\sin(sr)}{sr} r^2 dr \right]. \quad (2)$$

For the calculation of the SAXS intensity from a finite-size model, however, one must ensure that the size of the model is sufficiently large such that the relevant scattering region of

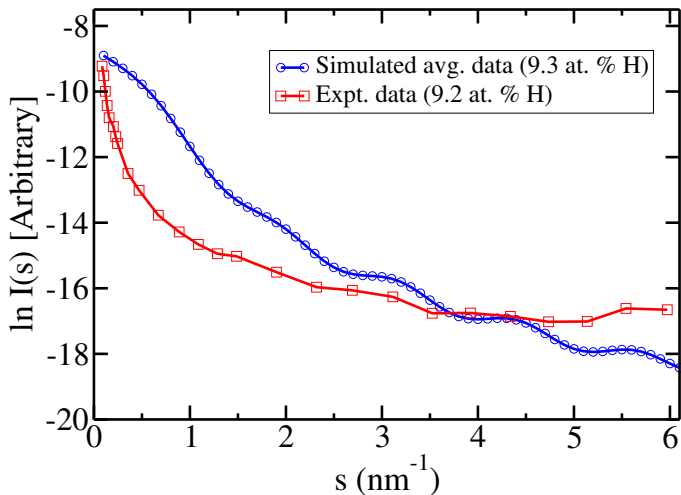


FIG. 6. (Color online) Simulated SAXS data for a model network of  $a$ -Si:H with 9.3 at. % H. Experimental data correspond to a sample of  $a$ -Si:H with 9.2 at. % H from Ref. 49.

interest  $s \approx 2\pi/D \gg s_{min} = 2\pi/L$ , where  $L$  and  $D$  are the linear size of the model and the lengthscale associated with the inhomogeneities to be measured, respectively. In actual calculations, Eq. 2 presents an additional complication due to the oscillatory nature of the integral with a finite upper limit due to the finite size of the models. Furthermore, since  $\sin(sr)/sr$  does not completely decay for  $sr = 2\pi$ , one should employ a somewhat larger value of  $s_{min}$  than  $2\pi/L$  for accurate simulations of SAXS data in this region. Given the modest size of our models and the uncertainty associated with neglecting the term involving  $\sin(sr)/sr$  and the oscillatory nature of the integral, we use Eq. 1 directly in our simulation and average the results by generating an ensemble of random scattering vectors distributed in a solid angle of  $4\pi$ . The atomic-scattering factors  $f_i$  for Si and H atoms have been obtained from the corresponding Cromer-Mann coefficients,[51] which accurately produce the data listed in the international tables for crystallography [52] for  $0 < \sin \theta/\lambda < 2.0 \text{ \AA}^{-1}$ . Debye corrections to the atomic-scattering factors are not included in this work.

Figure 6 shows the results from our simulations for a model amorphous-silicon network with 9.3 at. % H along with the experimental SAXS data reported in Ref. 49. For the purpose of comparison, we have rescaled the simulated data by a constant factor. The plot suggests that the simulated data agree with the experimental data qualitatively. The deviation from the experimental data can be attributed partly to the relatively modest size of the models, which makes it difficult to simulate the region with small values of  $s$ , and partly to the dependence of the experimental SAXS data on the method of sample preparation and condition. Since the typical linear size of the models in our work is of the order of  $L = 51 \text{ \AA}$ , the values of the intensity for the region below  $0.125 \text{ \AA}^{-1}$  have been affected by the finite-size effects. Wilkinson *et al.*[49] have observed that experimental SAXS data obtained for a number of device-quality  $a$ -Si:H samples, which were produced by a variety of methods, can vary considerably from

sample to sample depending upon the preparation condition of the samples. Thus, a quantitative comparison of simulated data from finite-size models with experimental SAXS data is highly nontrivial, and it requires large-scale simulations with models having a linear size of several tens of angstroms.

## V. CONCLUSIONS

In this paper, we have studied the morphology and microvoid distribution in large models of  $a$ -Si:H at low (8.3–9.3 at. % H) and high (18.3 at. % H) concentrations of hydrogen using a combination of *ab initio* total-energy relaxations and classical metadynamics simulations. The number density of microvoids,  $7\text{--}8 \times 10^{18} \text{ cm}^{-3}$ , calculated from our models with 8.3 at. % H is comparable with the experimental value of  $2\text{--}4 \times 10^{19} \text{ cm}^{-3}$  for device-quality samples obtained by combining results from SAXS and IR measurements, and  $1\text{--}3 \times 10^{18} \text{ cm}^{-3}$  estimated from hydrogen and implanted-helium effusion measurements. The linear size of the microvoids has been found to be in the range  $2.7\text{--}4.0 \text{ \AA}$ , which compares well with the experimental values,  $3.3\text{--}4.8 \text{ \AA}$ , observed from SAXS and PAS. Our results suggest that the morphology of microvoids at low concentration of hydrogen (below 10–12 at. % H) is dominated by an almost isolated distribution of small cavities, whereas at high concentration (near 18 at. % H or above) it comprises numerous interconnected cavities of non-spherical geometry. This observation is consistent with hydrogen and implanted-helium effusion measurements.

The work presented here has both direct and indirect impact on the development of new technologies in the area of low-power non-volatile memory and green energy from next-generation silicon-heterojunction solar cells. In a broader sense, the morphology and connectivity of void regions are widely believed to be the key to the fast ionic conduction in conductive bridging random access memory (CBRAM), which is based upon ultra-low-power resistive switching (RS) mechanisms. In CBRAM devices,[53, 54] the switching mechanism is achieved via the formation/dissolution of conducting filaments (CFs) upon small electrical stimulations. However, the morphology, atomistic growth, and the direction of CF formation are still unclear. While a growth direction from an inert cathode to an active (oxidizable) anode follows from the conventional electrochemical theory,[55] an opposite growth direction has been also reported in the literature [56, 57] and observed via *in situ* transmission electron microscopy (TEM).[58] This indicates that the morphology and growth dynamics of CFs not only depend on ion adsorption/desorption, metal-ion migration rate and electrochemistry, but also on the microstructure of the solid electrolyte under an electrical bias. A direct connection of our work to resistive RAM (ReRAM) devices follows from a recent study on  $\text{Al}/a\text{-SiN}_x\text{:H}/\text{p}^+\text{-Si}$  devices.[59] It has been observed that an RS mechanism with a very low programmable current can be obtained by varying the N/Si atomic ratio, where the low-resistance state corresponds to silicon dangling-bond conduction paths produced by electric-field-induced breaking of weak Si-H bonds and  $\text{H}^+$  ion migration. On the other hand,



the conduction in the high-resistance state is understood to be associated with the hopping transport or the Poole-Frenkel mechanism. We expect that our approach to a microstructural analysis of general glassy systems will greatly clarify the microscopic switching processes using first-principles calculations.

Our work is also particularly beneficial to the study of amorphous/crystalline interfaces for development of solar cells based upon *a*-Si:H/*c*-Si heterojunction intrinsic thin-layer (HIT) technology.[60] As noted earlier, despite decades of intensive research, the light-induced degradation of *a*-Si:H continues to pose a major problem in the development of stable high-yield *a*-Si:H-based solar cells. In view of this, much of the current works on silicon-based photovoltaic devices are now directed toward developing heterojunction technologies based on amorphous and crystalline Si interfaces. Panasonic Inc. has recently announced the availability of *a*-Si:H/*c*-Si HIT<sup>TM</sup> 300 cell modules (330 W),[61] which are more powerful than the conventional (260 W) *c*-Si-based solar cells. Further development in this area requires large-scale mod-

eling of *a*-Si:H/*c*-Si heterojunctions with a very low defect density. Since HIT cells are characterized by a layer of crystalline Si sandwiched between p- and n-doped *a*-Si:H, with a thin buffer layer of intrinsic *a*-Si:H between *c*-Si and doped *a*-Si:H surfaces, the metadynamical approach presented here provides a natural route to model such thin-layer heterojunctions and to study their photovoltaic properties. This paper points the way to implement such calculations for general amorphous/crystalline heterojunctions.

## VI. ACKNOWLEDGEMENTS

The work is partially supported by the US National Science Foundation (NSF) under grant numbers DMR 1507166, DMR 1507118 and DMR 1507670. We acknowledge the use of computing resources at the Texas Advanced Computing Center (TACC). D.P. acknowledges financial support from the NSF.

- 
- [1] J. Baum, K. K. Gleason, A. Pines, A. N. Garroway, and J. A. Reimer, "Multiple-quantum NMR study of clustering in hydrogenated amorphous silicon," *Phys. Rev. Lett.* **56**, 1377 (1986).
- [2] Y. Wu, J. T. S., D. X. Han, J. M. Rutland, R. S. Crandall, and A. H. Mahan, "New hydrogen distribution in *a*-Si:H: An NMR study," *Phys. Rev. Lett.* **77**, 2049 (1996).
- [3] K. K. Gleason, M. A. Petrich, and J. A. Reimer, "Hydrogen microstructure in amorphous hydrogenated silicon," *Phys. Rev. B* **36**, 3259 (1987).
- [4] C. Manfredotti, F. Fizzotti, M. Boero, P. Pastorino, P. Polesello, and E. Vittone, "Influence of hydrogen-bonding configurations on the physical properties of hydrogenated amorphous silicon," *Phys. Rev. B* **50**, 18046 (1994).
- [5] H. M. Branz, "Hydrogen collision model: Quantitative description of metastability in amorphous silicon," *Phys. Rev. B* **59**, 5498 (1999).
- [6] D. E. Carlson, "Hydrogenated microvoids and light-induced degradation of amorphous-silicon solar cells," *Appl. Phys. A* **41**, 305 (1986).
- [7] J. D. Ouwens and R. E. I. Schropp, "Hydrogen microstructure in hydrogenated amorphous silicon," *Phys. Rev. B* **54**, 17759 (1996).
- [8] S. Acco, D. L. Williamson, P. A. Stolk, F. W. Saris, M. J. van den Boogaard, W. C. Sinke, W. F. van der Weg, S. Roorda, and P. C. Zalm, "Hydrogen solubility and network stability in amorphous silicon," *Phys. Rev. B* **53**, 4415 (1996).
- [9] J. B. Boyce and M. Stutzmann, "Orientational ordering and melting of molecular H<sub>2</sub> in an *a*-Si matrix: NMR studies," *Phys. Rev. Lett.* **54**, 562 (1985).
- [10] H. V. Löhneysen, H. J. Schink, and W. Beyer, "Direct experimental evidence for molecular hydrogen in amorphous Si:H," *Phys. Rev. Lett.* **52**, 549 (1984).
- [11] J. E. Graebner, B. Golding, L. C. Allen, D. K. Biegelsen, and M. Stutzmann, "Solid hydrogen in hydrogenated amorphous silicon," *Phys. Rev. Lett.* **52**, 553 (1984).
- [12] Y. J. Chabal and C. K. N. Patel, "Molecular hydrogen in *a*-Si:H," *Rev. Mod. Phys.* **59**, 835 (1987).
- [13] S. Guha, J. Yang, S. J. Jones, Yan Chen, and D. L. Williamson, "Effect of microvoids on initial and lightdegraded efficiencies of hydrogenated amorphous silicon alloy solar cells," *Appl. Phys. Lett.* **61**, 1444 (1992).
- [14] X. Zou, Y. C. Chan, D. P. Webb, Y. W. Lam, Y. F. Hu, C. D. Belling, S. Fung, and H. M. Weng, "Photoinduced dehydrogenation of defects in undoped *a*-Si:H using positron annihilation spectroscopy," *Phys. Rev. Lett.* **84**, 769 (2000).
- [15] M. Fehr, A. Schnegg, B. Rech, O. Astakhov, F. Finger, R. Bittl, C. Teutloff, and K. Lips, "Metastable defect formation at microvoids identified as a source of light-induced degradation in *a*-Si:H," *Phys. Rev. Lett.* **112**, 066403 (2014).
- [16] A. H. Mahan, D. L. Williamson, B. P. Nelson, and R. S. Crandall, "Characterization of microvoids in device-quality hydrogenated amorphous silicon by small-angle X-ray scattering and infrared measurements," *Phys. Rev. B* **40**, 12024 (1989).
- [17] A.H. Mahan, D.L. Williamson, B.P. Nelson, and R.S. Crandall, "Small-angle X-ray scattering studies of microvoids in *a*-SiC:H and *a*-Si:H," *Sol. Cells* **27**, 465 (1989).
- [18] A. Laio and M. Parrinello, "Escaping free-energy minima," *Proc. Nat. Acad. Sci.* **99**, 12562 (2002).
- [19] W. Beyer, W. Hilgers, P. Prunici, and D. Lennartz, "Voids in hydrogenated amorphous silicon materials," *J. Non-Cryst. Solids* **358**, 2023 (2012).
- [20] W. Beyer, "Characterization of microstructure in amorphous and microcrystalline Si and related alloys by effusion of implanted helium," *Phys. Stat. Sol. (c)* **1**, 1144 (2004).
- [21] W. Beyer, D. Lennartz, P. Prunici, and H. Stiebig, "Annealing effects of microstructure in thin-film silicon solar cell materials measured by effusion of implanted rare gas atoms," *MRS Proc.* **1321**, mrss11-1321-a17-14 (2011).
- [22] S. Muramatsu, R. Suzuki, L. Wei, and S. Tanigawa, "Microvoids in *a*-Si:H and *a*-SiGe:H alloys," *Sol. Energ. Mat. Sol. Cells* **34**, 525 (1994).
- [23] A. Guinier, G. Fournet, C. B. Walker, and K. L. Yudowitch, *Small-Angle Scattering of X-Rays* (Wiley, New York, 1995).

- [24] D.L. Williamson, A.H. Mahan, B.P. Nelson, and R.S. Crandall, "The observation of microvoids in device quality hydrogenated amorphous silicon," *J. Non-Cryst. Solids* **114**, 226 (1989).
- [25] P. Biswas, R. Atta-Fynn, and D. A. Drabold, "Experimentally constrained molecular relaxation: The case of hydrogenated amorphous silicon," *Phys. Rev. B* **76**, 125210 (2007).
- [26] G. T. Barkema and N. Mousseau, "Event-based relaxation of continuous disordered systems," *Phys. Rev. Lett.* **77**, 4358 (1996).
- [27] A. Pandey, P. Biswas, and D. A. Drabold, "Force-enhanced atomic refinement: Structural modeling with interatomic forces in a reverse Monte Carlo approach applied to amorphous Si and SiO<sub>2</sub>," *Phys. Rev. B* **92**, 155205 (2015).
- [28] F. H. Stillinger and T. A. Weber, "Computer simulation of local order in condensed phases of silicon," *Phys. Rev. B* **31**, 5262 (1985).
- [29] A. Pandey, P. Biswas, and D. A. Drabold, "Inversion of diffraction data for amorphous materials," *Sci. Rep.* **6**, 33731 (2016).
- [30] K. Prasai, P. Biswas, and D. A. Drabold, "Sculpting the band gap: A computational approach," *Sci. Rep.* **5**, 15522 (2015).
- [31] P. Biswas, R. Atta-Fynn, and S. R. Elliott, "Metadynamical approach to the generation of amorphous structures: The case of *a*-Si:H," *Phys. Rev. B* **93**, 184202 (2016).
- [32] G. J. Martyna, M. E. Tuckerman, D. J. Tobias, and M. L. Klein, "Explicit reversible integrators for extended systems dynamics," *Mol. Phys.* **87**, 1117 (1996).
- [33] We have used a continuous atomic-neighbor function as a collective variable in this work. See Ref. 31 for details.
- [34] J. M. Soler, E. Artacho, J. D. Gale, A. Garcia, J. Junquera, P. Ordejón, and D. Sanchez-Portal, "The siesta method for ab initio order-*n* materials simulation," *J. Phys.: Condens. Matter* **14**, 2745 (2002).
- [35] J. P. Perdew and A. Zunger, "Self-interaction correction to density-functional approximations for many-electron systems," *Phys. Rev. B* **23**, 5048 (1981).
- [36] N. Troullier and José Luís Martins, "Efficient pseudopotentials for plane-wave calculations," *Phys. Rev. B* **43**, 1993 (1991).
- [37] Leonard Kleinman and D. M. Bylander, "Efficacious form for model pseudopotentials," *Phys. Rev. Lett.* **48**, 1425 (1982).
- [38] O. F. Sankey and D. J. Niklewski, "*Ab initio* multicenter tight-binding model for molecular-dynamics simulations and other applications in covalent systems," *Phys. Rev. B* **40**, 3979 (1989).
- [39] J. Harris, "Simplified method for calculating the energy of weakly interacting fragments," *Phys. Rev. B* **31**, 1770 (1985).
- [40] D.A. Drabold, T.A. Abteu, F. Inam, and Y. Pan, "Network structure and dynamics of hydrogenated amorphous silicon," *J. Non-Cryst. Solids* **354**, 2149 (2008).
- [41] P. Biswas, D. A. Drabold, and R. Atta-Fynn, "Microstructure from joint analysis of experimental data and ab initio interactions: Hydrogenated amorphous silicon," *J. Appl. Phys.* **116**, 244305 (2014).
- [42] P. Biswas and R. Timilsina, "Vacancies, microstructure and the moments of nuclear magnetic resonance: The case of hydrogenated amorphous silicon," *J. Phys.: Condens. Matter* **23**, 065801 (2011).
- [43] P. Biswas and S. R. Elliott, "Nanoscale structure of microvoids in *a*-Si:H: A first-principles study," *J. Phys.: Condens. Matter* **27**, 435201 (2015).
- [44] The  $L^1$  norm or distance between two vectors,  $\mathbf{p}$  and  $\mathbf{q}$ , in  $n$ -dimensional space is given by,  $R_L = \|\mathbf{p} - \mathbf{q}\| = \sum_{i=1}^n |p_i - q_i|$ . This is also known as the Manhattan distance, and is particularly useful to calculate distances between two points in a grid-based geometrical arrangement.
- [45] C. C. Griffioen, J. H. Evans, P. C. De Jong, and A. Van Veen, "Helium desorption/permeation from bubbles in silicon: A novel method of void production," *Nucl. Instrum. Methods Phys. Res., Sect. B* **27**, 417 (1987).
- [46] While a small value of  $\Delta x$  is useful for an accurate construction of the shape of microvoids at high resolution, it may introduce artificial lacunal structure in the resulting void distribution. In contrast, a large value of  $\Delta x$  may reduce the spatial resolution and, thus, washes out some details of the surface structure of the voids.
- [47] L. A. Feigin and D. I. Svergun, *Structure Analysis by Small-Angle X-Ray and Neutron Scattering* (Springer Science+Business Media, New York, 1987).
- [48] In the presence of periodic boundary conditions, the distance between two atoms depends on both  $r_i$  and  $r_j$  and the linear size of the model. In this case, the double sum in Eq. 1 cannot be replaced by the square of a single sum, and a direct evaluation of Eq. 1 requires  $(N^2MK)/2$  operations, where  $N$  is the number of atoms,  $M$  is the number of unit scattering vectors needed for configuration averaging, and  $K$  is the number of different magnitudes of the scattering vectors. For  $N=5000$ ,  $M=1000$ , and  $K=100$ , this corresponds to trillions of floating-point operations, which translate into several tens of hours of CPU time in a standard desktop workstation.
- [49] D. L. Williamson, S. Jones, and Y. Chen, *Small-Angle X-Ray Scattering Studies of Microvoids in Amorphous-Silicon-Based Semiconductors* (Technical Report: NREL/TP-411-6855, National Renewable Energy Laboratory, 1994).
- [50] F. Zernike and J. A. Prins, "Die beugung von röntgenstrahlen in flüssigkeiten als effekt der molekülordnung," *Z. Phys. A* **41**, 184 (1927).
- [51] D. T. Cromer and J. B. Mann, "Compton scattering factors for spherically symmetric free atoms," *J. Chem. Phys.* **47**, 1892 (1967).
- [52] E. Prince, ed., *International Tables for Crystallography* (Kluwer Academic Publishers, Dordrecht, The Netherlands, 2004).
- [53] M. N. Kozicki and H. J. Barnaby, "Conductive bridging random access memory materials, devices and applications," *Semicond. Sci. Technol.* **31**, 113001 (2016).
- [54] M. N. Kozicki and W. C. West, "Programmable metallization cell structure and method of making same," US Patent, 5761115.
- [55] R. Waser and Masakazu A., "Nanoionics-based resistive switching memories," *Nat. Mater.* **6**, 833 (2007).
- [56] Y. Yang, Peng G., Siddharth G., Ting C., X. Pan, and W. Lu, "Observation of conducting filament growth in nanoscale resistive memories," *Nat. Commun.* **3**, 732 (2012).
- [57] S. Gao, C. Song, C. Chen, F. Zeng, and F. Pan, "Dynamic processes of resistive switching in metallic filament-based organic memory devices," *J. Phys. Chem. C* **116**, 17955 (2012).
- [58] Qi Liu, Jun Sun, Hangbing Lv, Shibing Long, Kuibo Yin, Neng Wan, Yingtao Li, Litao Sun, and Ming Liu, "Real-time observation on dynamic growth/dissolution of conductive filaments in oxide-electrolyte-based ReRAM," *Adv. Mater.* **24**, 1844 (2012).
- [59] X. Jiang, Z. Ma, J. Xu, K. Chen, L. Xu, W. Li, X.n Huang, and D. Feng, "*a*-SiN<sub>x</sub>:H-based ultra-low power resistive random access memory with tunable Si dangling bond conduction paths," *Sci. Rep.* **5**, 15762 (2015).
- [60] T. Mishima, M. Taguchi, H. Sakata, and E. Maruyama, "Development status of high-efficiency HIT solar cells," *Sol. Energ. Mat. Sol. Cells* **95**, 18 (2011), 19th International Photovoltaic Science and Engineering Conference and Exhibition (PVSEC-

19) Jeju, Korea, 9-13 November 2009.

[61] M. Taguchi, A. Yano, S. Tohoda, K. Matsuyama, Y. Nakamura, T. Nishiwaki, K. Fujita, and E. Maruyama, "24.7% record efficiency HIT solar cell on thin silicon wafer," *IEEE J. Photovolt.* **4**, 96 (2014).